

# Non-perturbative interpretation of the Bloch vector's path beyond rotating wave approximation

Giuliano Benenti,<sup>1,2</sup> Stefano Succi,<sup>3</sup> and Giuliano Strini<sup>4</sup>

<sup>1</sup>*CNISM and Center for Nonlinear and Complex Systems,*

*Università degli Studi dell'Insubria, via Valleggio 11, 22100 Como, Italy*

<sup>2</sup>*Istituto Nazionale di Fisica Nucleare, Sezione di Milano, via Celoria 16, 20133 Milano, Italy*

<sup>3</sup>*Department of Information Technologies, University of Milan, via Bramante 65, 26013 Crema, Italy*

<sup>4</sup>*Department of Physics, University of Milan, via Celoria 16, 20133 Milano, Italy*

The Bloch vector's path of a two-level system exposed to a monochromatic field exhibits, in the regime of strong coupling, complex corkscrew trajectories. By considering the infinitesimal evolution of the two-level system when the field is treated as a classical object, we show that the Bloch vector's rotation speed oscillates between zero and twice the rotation speed predicted by the rotating wave approximation. Cusps appear when the rotation speed vanishes. We prove analytically that in correspondence to cusps the curvature of the Bloch vector's path diverges. On the other hand, numerical data show that the curvature is very large even for a quantum field in the deep quantum regime with mean number of photons  $\bar{n} \lesssim 1$ . We finally compute numerically the typical error size in a quantum gate when the terms beyond rotating wave approximation are neglected.

PACS numbers: 42.50.Pq, 03.67.-a

## I. INTRODUCTION

The dynamics of two-level systems in an external field has been thoroughly studied for years. This problem appears in several physical systems and is significant for the realization of quantum gates [1, 2]. The model consists of the Hamiltonian of a two-level system, coupled to a classical field or to a quantum harmonic oscillator. There are no general methods for solving analytically these models without any approximations, so several approaches have been used to study their behavior. The best known is the Rotating Wave Approximation (RWA), that consists in neglecting the effects of the rapidly rotating terms [3].

For an atom residing in a resonant cavity the frequency  $\Omega$  of the Rabi oscillations between the two relevant states of the atom is typically  $10^{-6}$  of the atomic frequency  $\omega_a$  and of the cavity frequency  $\omega$ , so that the RWA yields a good description of the system [4]. On the other hand, in circuit quantum electrodynamics (cQED) [5, 6], where superconducting qubits play the role of artificial atoms, one can enter the so-called ultrastrong coupling regime in which the ratio  $\Omega/\omega > 0.1$  [7–9] (at resonance,  $\omega_a = \omega$ ). In this regime, effects beyond RWA should be taken into account, both for the dynamics of pure states [10–15] and for dissipative dynamics [16–18].

The consideration of high Rabi frequencies is natural in quantum information theory, since high speed operations are needed to perform a large number of quantum gates within the decoherence time scale, an unavoidable request for fault tolerant quantum computation [1, 2]. Therefore, a deeper understanding of the effects beyond RWA is relevant for the prospects of quantum computation.

In this paper, we explain, in a non-perturbative manner, the non-trivial Bloch vector's path of a two-level system exposed to a monochromatic field. By considering the infinitesimal evolution of the state vector, we

determine the temporal dependence of the rotation axis and frequency. In particular, we show analytically that, when the field is treated as a classical object, the rotation frequency oscillates between zero and twice the value predicted by the RWA. The vanishing of the rotation frequency is associated with cusps in the Bloch vector's path. Correspondingly, the curvature of the Bloch vector's trajectory diverges. On the other hand, we show numerically that the curvature can take very large values even for a quantum field in the deep quantum regime with mean number of photons  $\bar{n} \lesssim 1$ . We finally show numerically that the size of the errors induced in a quantum gate by the terms beyond RWA scales as  $1/\omega$ .

The paper is organized as follows. The model for a two-level system in a classical field is introduced and studied numerically in Sec. II, while the analytical interpretation of the Bloch vector's paths is reported in Sec. III. Numerical results for the quantum field model are shown in Sec. IV, where the errors introduced by the terms beyond RWA are also investigated. We finish with concluding remarks in Sec. V.

## II. THE CLASSICAL FIELD MODEL

We consider the following time-dependent Hamiltonian  $H(t)$ , describing the interaction of a two-level system with a classical monochromatic field (we set  $\hbar = 1$ ):

$$H(t) = H_0 + H_I(t),$$

$$H_0 = \epsilon_0|0\rangle\langle 0| + \epsilon_1|1\rangle\langle 1|, \quad (1)$$

$$H_I(t) = 2\Omega \cos(\omega t)(|0\rangle\langle 1| + |1\rangle\langle 0|),$$

where  $\omega$  is the frequency of the field and  $\Omega$  the (Rabi) frequency of the field-induced oscillations between the

two levels  $|0\rangle$  and  $|1\rangle$  [19]. The time evolution of the two-level state vector  $|\psi(t)\rangle = C_0(t)|0\rangle + C_1(t)|1\rangle$  is, in the interaction picture, governed by the equations

$$\begin{cases} i\dot{C}_0(t) = \Omega \left[ e^{i(\omega-\omega_a)t} + e^{-i(\omega+\omega_a)t} \right] C_1(t), \\ i\dot{C}_1(t) = \Omega \left[ e^{i(\omega+\omega_a)t} + e^{-i(\omega-\omega_a)t} \right] C_0(t), \end{cases} \quad (2)$$

where  $\omega_a = \epsilon_1 - \epsilon_0$  ( $\epsilon_1 > \epsilon_0$ ).

The terms depending on  $\omega + \omega_a$  oscillate very rapidly and are neglected in the rotating wave approximation. In this paper, we will explore the effects of these terms beyond RWA on the evolution of the two-level state vector  $|\psi(t)\rangle$ . For the sake of simplicity, we set the detuning  $\Delta = \omega - \omega_a = 0$ , as the treatment for  $\Delta \neq 0$  would be essentially identical to that for  $\Delta = 0$ . Finally, it is convenient to normalize time in units of the Rabi frequency, that is, we set  $\Omega = 1$ . Hence, we obtain

$$\begin{cases} i\dot{C}_0 = (1 + e^{-2i\omega t}) C_1, \\ i\dot{C}_1 = (1 + e^{2i\omega t}) C_0. \end{cases} \quad (3)$$

The RWA approximation is valid when  $\omega \gg \Omega$  (in our units, when  $\omega \gg 1$ ).

A convenient geometric picture of the evolution of the state vector is provided by the Bloch ball representation [1, 2], with the Bloch coordinates defined as

$$\begin{cases} X = 2C_{0r}C_{1r} + 2C_{0i}C_{1i}, \\ Y = 2C_{0r}C_{1i} - 2C_{0i}C_{1r}, \\ Z = 2C_{0r}^2 + 2C_{0i}^2 - 1, \end{cases} \quad (4)$$

where  $C_{kr}$  and  $C_{ki}$  denote the real and imaginary parts of  $C_k$  ( $k = 0, 1$ ). The normalization constraint  $|C_0|^2 + |C_1|^2 = 1$  implies that the motion of the Bloch vector  $\mathbf{R} = (X, Y, Z)$  takes place on the unit (Bloch) sphere  $X^2 + Y^2 + Z^2 = 1$ .

The most interesting feature the Bloch vector's path is the presence of cusps, shown in Fig. 1. The corkscrew trajectories shown in this figure are obtained from numerical integration of the differential equations (3), starting from the initial condition  $C_0(0) = 1$ ,  $C_1(0) = 0$  (north pole of the Bloch sphere). The plots of Fig. 1 show, from top to bottom, the Bloch vector's trajectory and its projections on the  $YZ$ ,  $XZ$ , and  $XY$  planes; from left to right,  $\omega = 2.5, 5, 20$ , and RWA approximation ( $\omega \rightarrow \infty$ ). While within RWA the trajectory is a circle, corresponding to Rabi oscillations between states  $|0\rangle$  and  $|1\rangle$  (north and south pole of the Bloch sphere, respectively), cusps appear beyond RWA. We will interpret in a simple but exact manner these numerical results in Sec. III.

### III. INTERPRETATION OF THE BLOCH VECTOR'S PATH

We consider the infinitesimal evolution of the state vector:

$$|\psi(t+dt)\rangle = U(t, t+dt)|\psi(t)\rangle, \quad (5)$$

where the unitary operator  $U(t, t+dt)$  represents an infinitesimal rotation of the Bloch vector through an angle  $d\theta$  about the axis directed along the unit vector  $\hat{\mathbf{n}} = (n_X, n_Y, n_Z)$ :

$$U(t, t+dt) = \left( I - i \frac{d\theta}{2} \hat{\mathbf{n}} \cdot \boldsymbol{\sigma} \right), \quad (6)$$

where  $I$  is the identity operator and  $\boldsymbol{\sigma} = (\sigma_X, \sigma_Y, \sigma_Z)$ ,  $\sigma_k$  ( $k = X, Y, Z$ ) being the Pauli operators. In the  $\{|0\rangle, |1\rangle\}$  basis, Eq. (5) reads as follows:

$$\begin{aligned} & \begin{bmatrix} C_0(t+dt) \\ C_1(t+dt) \end{bmatrix} \\ &= \begin{bmatrix} 1 - in_Z \frac{d\theta}{2} & -(n_Y + in_X) \frac{d\theta}{2} \\ (n_Y - in_X) \frac{d\theta}{2} & 1 + in_Z \frac{d\theta}{2} \end{bmatrix} \begin{bmatrix} C_0(t) \\ C_1(t) \end{bmatrix}. \end{aligned} \quad (7)$$

Since

$$|\psi(t+dt)\rangle = |\psi(t)\rangle + |\dot{\psi}(t)\rangle dt, \quad (8)$$

with  $|\dot{\psi}(t)\rangle$  obtained from Eq. (3), we have

$$\begin{aligned} & \begin{bmatrix} C_0(t+dt) \\ C_1(t+dt) \end{bmatrix} \\ &= \begin{bmatrix} 1 & -i(1 + e^{-2i\omega t}) \\ -i(1 + e^{2i\omega t}) & 1 \end{bmatrix} \begin{bmatrix} C_0(t) \\ C_1(t) \end{bmatrix}. \end{aligned} \quad (9)$$

From comparison between Eqs. (7) and (9) we obtain

$$\begin{cases} n_X \frac{d\theta}{2} = [1 + \cos(2\omega t)]dt, \\ n_Y \frac{d\theta}{2} = \sin(2\omega t)dt, \\ n_Z = 0. \end{cases} \quad (10)$$

From the first two equations of this system we have

$$\dot{\theta} = \frac{d\theta}{dt} = 4|\cos(\omega t)|. \quad (11)$$

Therefore, the rotation speed  $\dot{\theta}$  vanishes when  $\cos(\omega t) = 0$ , that is, for

$$t = t_k = \frac{(2k+1)\pi}{2\omega}, \quad (k = 0, 1, \dots). \quad (12)$$

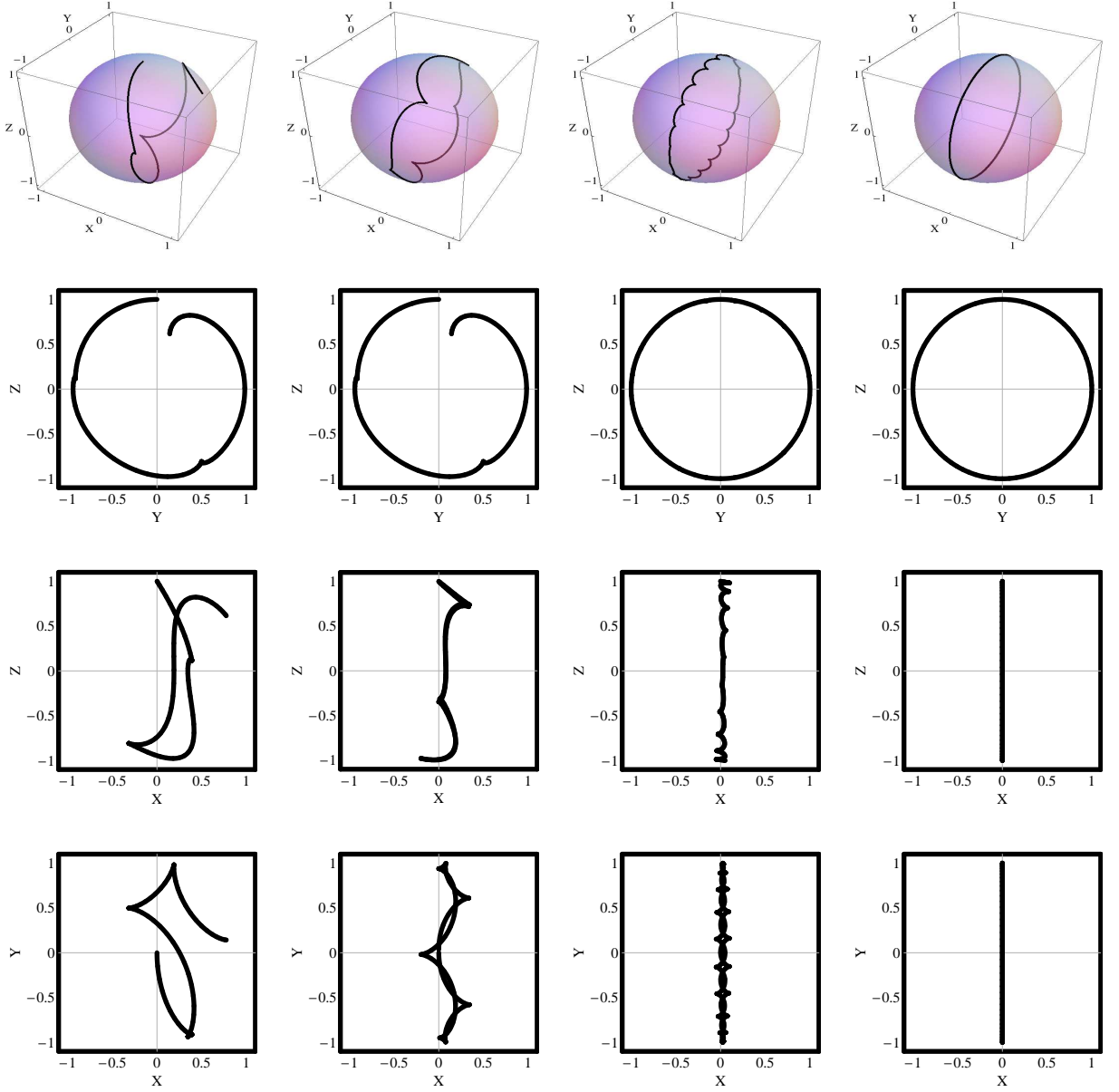


FIG. 1. Bloch vector's path (top plots) and its projections on, from the second to the fourth row, the  $YZ$ ,  $XZ$ , and  $XY$  planes. From left to right:  $\omega = 2.5, 5, 20$ , and RWA ( $\omega \rightarrow \infty$ ). Time evolution is followed, starting from the north pole, up to time  $\pi$  (within RWA, at such time the Bloch vector returns, for the first time, back to the north pole).

After insertion of Eq. (11) into Eq. (10), we obtain

$$\begin{cases} n_X = |\cos(\omega t)|, \\ n_Y = \sin(\omega t) \operatorname{sgn}[\cos(\omega t)], \\ n_Z = 0, \end{cases} \quad (13)$$

where  $\operatorname{sgn}(x) = x/|x|$  is the sign function. Therefore, at times  $t_k$  the rotation axis changes instantaneously from  $(n_X, n_Y, n_Z) = (0, 1, 0)$  to  $(0, -1, 0)$ , that is, from the  $Y$  axis to the opposite direction  $-Y$ . Such discontinuity in the rotation axis is associated with a cusp in the Bloch vector's path. As discussed in appendix A, the curvature

of the Bloch vector's path diverges at the cusps.

The dependence of the rotation axis and speed on time can be visualized by means of the schematic drawing in Fig. 2. Within RWA, the rotation speed is given by the length  $\dot{\theta}_{\text{RWA}} = 2\Omega = 2$  ( $\Omega = 1$  in our units) of the segment  $OA$  and the rotation axis is the  $X$  axis. On the other hand, when effects beyond RWA are taken into account, the rotation speed at time  $t$  is given by the length  $\dot{\theta} = 4|\cos(\omega t)|$  of the segment  $OB$ , and the rotation axis is directed along  $OB$ . Therefore, the rotation speed oscillates between  $\dot{\theta} = 0$  (at times  $t_k$ ) and  $\dot{\theta} = 4 = 2\dot{\theta}_{\text{RWA}}$  (at times  $\tilde{t}_k = k\pi/\omega$ ,  $k = 0, 1, \dots$ ).

In Fig. 3, we show the  $XY$ -plane projection of the

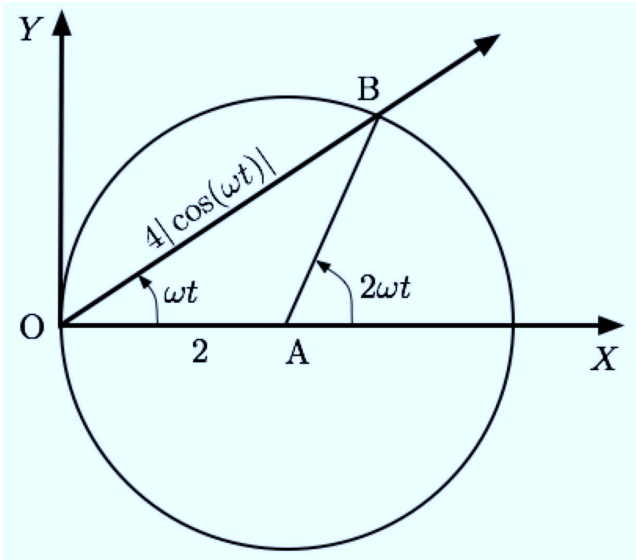


FIG. 2. Schematic illustration of the rotation axis and speed within and beyond RWA.

Bloch vector's evolution in the neighborhood of a cusp and compare it with the RWA approximation. It is interesting to remark that the distance between the two evolutions, shown at different times by dashed lines, is not simply given by the shortest distance between the exact trajectory and its RWA. This is due to the fact that, as pointed out above, while the RWA predicts a constant rotation velocity  $\dot{\theta}_{\text{RWA}} = 2$ , the exact evolution exhibits a variable rotation speed  $\dot{\theta} = 4|\cos(\omega t)|$ , which is faster than in the RWA far from the cusp and slows down up to  $\dot{\theta} = 0$  at the cusps.

The above discussed non-trivial behavior of the Bloch vector's path implies, as shown in Fig. 4, the existence of plateaus in the dependence of the path length  $s(t)$  as a function of time. The plateaus are obtained around the times  $t_k$  where the curvature of the Bloch vector's path diverges. The slope of  $s(t)$  oscillates between zero (at the cusps) and  $2\dot{\theta}_{\text{RWA}} = 4$ . Note that the overall path length is larger than within RWA, since the Bloch vector moves along a path longer than within RWA (see Fig. 3). The mean slope of  $s(t)$  approaches the RWA slope in the limit  $\omega \rightarrow \infty$ .

Finally, we point out that, while the curvature exhibits a singularity at the cusps, the functions  $X(t)$ ,  $Y(t)$ , and  $Z(t)$  are regular at the times  $t = t_k$  corresponding to such cusps. This is due to the fact that, as discussed above, the rotation speed tends to zero when  $t \rightarrow t_k$  [20].

#### IV. THE QUANTUM FIELD MODEL

The interaction between a two-level system and a single mode of the quantized electromagnetic field is de-

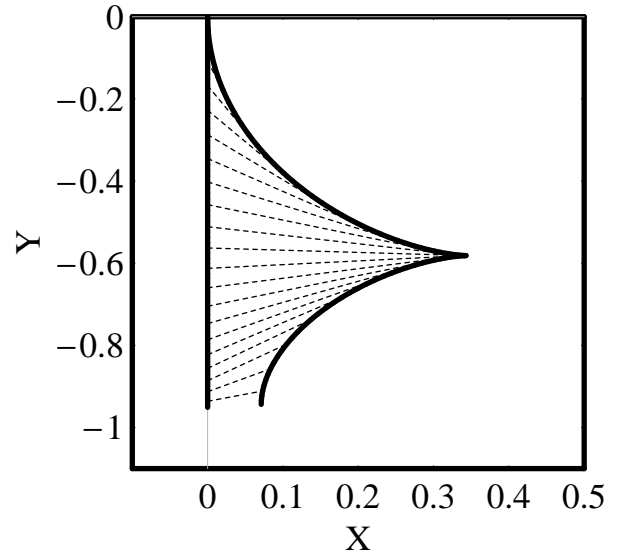


FIG. 3. Comparison between the XY projection of the Bloch vector's exact evolution (full curve) and its RWA (straight line) in the vicinity of a cusp, for  $\omega = 5$ . The dashed lines link points corresponding to the exact and approximate Bloch vectors,  $\mathbf{R}(t)$  and  $\mathbf{R}_{\text{RWA}}(t)$ , obtained after the same evolution time  $t$  (the different dashed lines correspond to different values of  $t$ ).

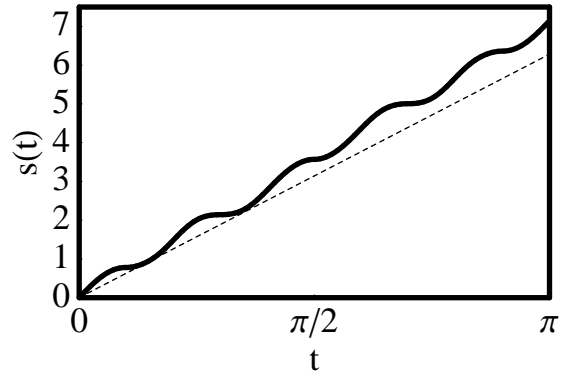


FIG. 4. Plateaus in the path length  $s(t)$  as a function of time (full curve), for  $\omega = 5$ . The straight dashed line corresponds to the RWA result,  $s(t) = 2t$ .

scribed by the Hamiltonian ( $\hbar = 1$ ) [3]

$$H = H_0 + H_I,$$

$$H_0 = \frac{1}{2} \omega_a \sigma_Z + \omega \left( a^\dagger a + \frac{1}{2} \right), \quad (14)$$

$$H_I = \lambda \sigma_+ (a^\dagger + a) + \lambda^* \sigma_- (a^\dagger + a),$$

where  $\sigma_\pm = \frac{1}{2}(\sigma_X \pm i\sigma_Y)$  are the rising and lowering operators for the two-level system:  $\sigma_+|0\rangle = |1\rangle$ ,  $\sigma_+|1\rangle = 0$ ,  $\sigma_-|0\rangle = 0$ ,  $\sigma_-|1\rangle = |0\rangle$ , the operators  $a^\dagger$  and  $a$  create and annihilate a photon:  $a^\dagger|n\rangle_p = \sqrt{n+1}|n+1\rangle_p$ ,

$a|n\rangle_p = \sqrt{n}|n-1\rangle_p$ ,  $|n\rangle_p$  being the Fock state with  $n$  photons. For simplicity's sake, we consider the resonant case ( $\omega = \omega_a$ ) and the coupling constant  $\lambda \in \mathbb{R}$ . The RWA is obtained when we neglect the term  $\sigma_+ a^\dagger$ , which simultaneously excites the two-level system and creates a photon, and  $\sigma_- a$ , which de-excites the two-level system and annihilates a photon. In this limit, Hamiltonian (14) reduces to the Jaynes-Cummings Hamiltonian (see, for instance, Ref. [3]). Within RWA (Jaynes-Cummings limit), there are coherent Rabi oscillations between the two-level system-cavity states  $|0\rangle|n+1\rangle_p$  and  $|1\rangle|n-1\rangle_p$ . The frequency of such oscillations is  $\Omega_n = \lambda\sqrt{n}$ .

We study numerically the temporal evolution of the two-level system's state vector, when the initial state is  $|\phi_0\rangle|\alpha\rangle_p$ , where  $|\phi_0\rangle = \cos(\frac{\theta}{2})|0\rangle + \sin(\frac{\theta}{2})|1\rangle$  is the initial state of the two-level system and  $|\alpha\rangle_p = \sum_{n=0}^{\infty} c_n|n\rangle_p$ , with  $c_n = \exp(-\frac{1}{2}|\alpha|^2) \frac{\alpha^n}{\sqrt{n!}}$ , is the coherent state of the field, with mean number of photons given by  $\bar{n} = |\alpha|^2$  and root mean square deviation in the photon number  $\Delta n = \sqrt{\bar{n}}$ . The classical field limit is obtained for  $\bar{n} \rightarrow \infty$ , with constant  $\Omega_{\bar{n}} = \lambda\sqrt{\bar{n}} = \lambda\alpha$ , that is, with  $\lambda \propto 1/\alpha$ . We measure frequencies in units of  $\Omega_{\bar{n}}$ , namely we set  $\Omega_{\bar{n}} = 1$ , i.e.,  $\lambda = 1/\alpha$ .

We focus on the time evolution of the Bloch ball coordinates. In Fig. 5 we show the Bloch vector's trajectory and its projection on the  $YZ$ ,  $XZ$ , and  $XY$  planes, both in the deep quantum regime  $\alpha = 1$  (first two columns in Fig. 5) and closer to the classical field limit ( $\alpha = 5$ , corresponding to  $\bar{n} = 25$  photons, in the third column of Fig. 5). For small values of  $\alpha$  the Bloch vector's path crucially depends on the initial state  $|\phi_0\rangle$  of the two-level system, as we can see from the two cases shown in Fig. 5:  $\theta = 0$  (north pole of the Bloch sphere) and  $\theta = \pi$  (south pole) (such strong dependence does not appear for large values of  $\alpha$ ). In all instances,  $\omega = 5$ , so that the effects beyond RWA are pronounced. The plots for  $\alpha = 5$  are quite close to the classical field plots (fourth column in Fig. 5). On the other hand, cusps, even though smoothed, are very pronounced even in the deep quantum regime  $\alpha = 1$ . In Table I we show the value of the curvature  $\kappa$  at times  $t_1 = \frac{\pi}{2\omega}$  and  $t_2 = \frac{3\pi}{2\omega}$ , where  $\kappa$  diverges for the classical field model (see appendix A). Note that the obtained values are much larger than the value  $\kappa = 1$  corresponding to RWA in the classical field model.

	first peak	second peak
$\alpha = 1, \theta = 0$	$2.6 \times 10^4$	$1.8 \times 10^2$
$\alpha = 1, \theta = \pi$	12	8.5
$\alpha = 5, \theta = 0$	$1.5 \times 10^5$	$2.8 \times 10^3$

TABLE I. Value of the curvature  $\kappa$  for the first two peaks, at times  $t_1 = \frac{\pi}{2\omega}$  and  $t_2 = \frac{3\pi}{2\omega}$  where  $\kappa$  diverges when the field is treated as a classical object. The three lines of this table correspond to the first three columns of Fig. 5, so that  $\omega = 5$ .

We finally estimate the error introduced by the terms

beyond RWA in a typical quantum gate. Since the time elapsed during an elementary quantum gate is of the order of the inverse of the Rabi frequency, we compute the Euclidean square distance on the Bloch ball between the exact and the RWA evolution,

$$\|\mathbf{R} - \mathbf{R}_{\text{RWA}}\| = \sqrt{(X - X_{\text{RWA}})^2 + (Y - Y_{\text{RWA}})^2 + (Z - Z_{\text{RWA}})^2} \quad (15)$$

as a function of time, up to  $t = \tau = \pi/\Omega$ . The root mean square

$$\delta = \sqrt{\frac{1}{\tau} \int_0^\tau dt \|\mathbf{R}(t) - \mathbf{R}_{\text{RWA}}(t)\|^2} \quad (16)$$

indicates the typical size of the errors introduced in a quantum gate by the terms beyond RWA, once such terms are neglected. Our numerical data shown in Fig. 6 show that  $\delta \propto 1/\omega$  for any value of  $\alpha$ . Moreover, the values obtained for a quantum treatment of the field approach quite quickly the expectation of the classical field model, and already for  $\alpha = 5$  we obtain values of  $\delta$  close to the classical values.

## V. CONCLUSIONS

In this paper, we have explained features beyond RWA of the Bloch vector's path of a two-level system exposed to a monochromatic field, including the oscillation of the rotation frequency and axis and the presence of cusps in the trajectory. Our exact and non-perturbative analysis is based on the infinitesimal evolution of the two-level system state vector.

The above non-trivial features of the Bloch vector's path should be taken into account, together with the effects of noise, in any implementation of quantum gates, where error rates smaller than  $10^{-4}$  are requested for fault-tolerant quantum computation. In particular, since cusps are clearly seen even for the quantum field in the deep quantum regime with a small mean number of photons  $\bar{n} \lesssim 1$ , they should be relevant and observable in circuit QED experiments. The numerical results of Fig. 6 show that neglecting the terms beyond RWA one introduces an error of the order of the inverse of the ratio between the field and the Rabi frequency. Therefore, to obtain error rates smaller than  $10^{-4}$ , effects beyond RWA should be necessarily taken into account when  $\Omega/\omega > 10^{-4}$ , a limit largely overtaken in the ultrastrong in which the ratio  $\Omega/\omega > 0.1$ . Finally, the existence of cusps due to the presence of two frequencies, in this case  $\omega - \omega_a$  and  $\omega + \omega_a$ , appears as a rather general phenomenon, so that we expect cusps to appear in protocols such as the Raman transition [21]. This remains to be analyzed in future [22].

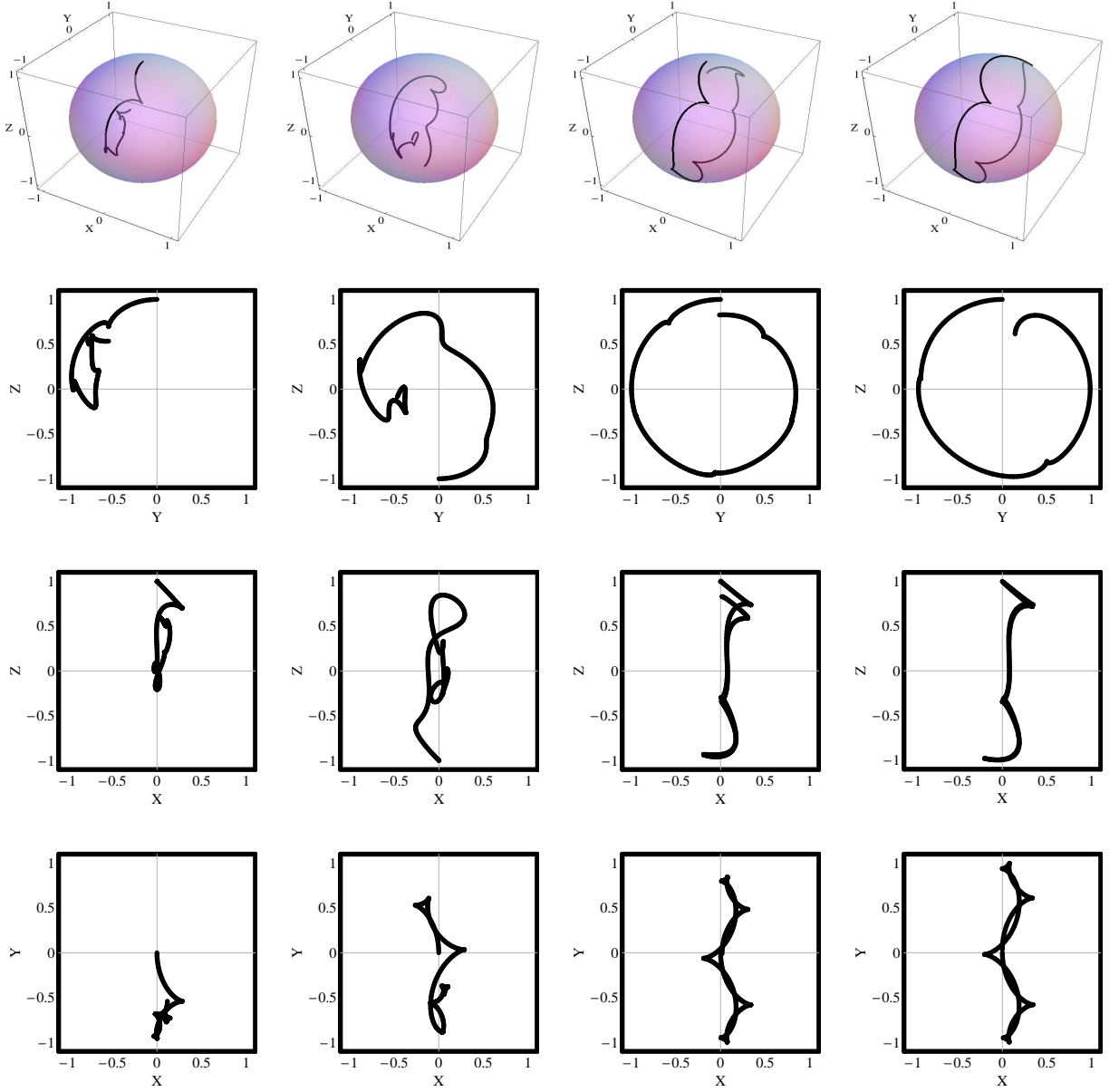


FIG. 5. Bloch vector's path (top plots) and its projections on, from the second to the fourth row, the  $YZ$ ,  $XZ$ , and  $XY$  planes. From left to right:  $\alpha = 1, \theta = 0$ ;  $\alpha = 1, \theta = \pi$ ;  $\alpha = 5, \theta = 0$ ; and classical field,  $\theta = 0$ . In all instances,  $\omega = 5$  and time evolution is followed up to time  $\pi$ .

#### Appendix A: Curvature of the Bloch vector's path

Given a point  $\mathbf{R} = (X, Y, Z)$  of the Bloch vector's trajectory, we compute its velocity as

$$\mathbf{V} = \dot{\mathbf{R}} = \mathbf{R} \times \dot{\theta} \hat{\mathbf{n}}, \quad (\text{A1})$$

with  $\hat{\mathbf{n}} = (n_X, n_Y, n_Z)$  direction of the rotation axis and  $\dot{\theta}$  rotation frequency. After substitution of Eqs. (11) and

(13) into (A1), we obtain the components of vector  $\vec{V}$ :

$$\begin{cases} V_X = -4Z \sin(\omega t) \cos(\omega t), \\ V_Y = 4Z \cos^2(\omega t), \\ V_Z = 4 \cos(\omega t) [X \sin(\omega t) - Y \cos(\omega t)]. \end{cases} \quad (\text{A2})$$

We then compute the tangent vector

$$\hat{\mathbf{t}} = \frac{d\mathbf{R}}{ds} = \frac{\mathbf{V}}{s}, \quad (\text{A3})$$

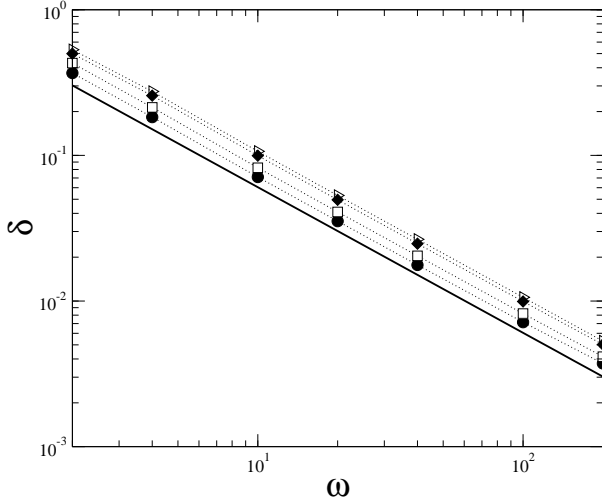


FIG. 6. Root mean square distance between the exact evolution and the RWA, for, from bottom to top,  $\alpha = 1$  (circles), 2 (squares), 5 (diamonds) and classical field (triangles). The straight full line shows the  $1/\omega$  slope.

where  $s$  is the arc length along the Bloch vector's path and

$$\dot{s} = |\dot{\mathbf{V}}| = 4|\cos(\omega t)|\sqrt{Z^2 + [X\sin(\omega t) - Y\cos(\omega t)]^2}. \quad (\text{A4})$$

Finally, the curvature of the Bloch vector's trajectory

is given by

$$\kappa = \left| \frac{d\hat{\mathbf{t}}}{ds} \right| = \frac{|\ddot{\mathbf{R}} - \dot{s}\hat{\mathbf{t}}|}{(\dot{s})^2}, \quad (\text{A5})$$

with the components  $(A_X, A_Y, A_Z)$  of the acceleration  $\mathbf{A} = \ddot{\mathbf{R}}$  given by

$$\begin{cases} A_X = -4Z\omega \cos(2\omega t), \\ A_Y = -4Z\omega \sin(2\omega t), \\ A_Z = 4\omega [X \cos(2\omega t) + Y \sin(2\omega t)], \end{cases} \quad (\text{A6})$$

and

$$\begin{aligned} \ddot{s} = 4 \left( \frac{d}{dt} |\cos(\omega t)| \right) \sqrt{Z^2 + [X \sin(\omega t) - Y \cos(\omega t)]^2} \\ + \frac{4|\cos(\omega t)|}{\sqrt{Z^2 + [X \sin(\omega t) - Y \cos(\omega t)]^2}} \\ \times \frac{\omega}{2} [(X^2 - Y^2) \sin(2\omega t) + XY \cos(2\omega t)]. \end{aligned} \quad (\text{A7})$$

As shown in Fig. 7, the curvature diverges at the times  $t_k$  of Eq. (12), corresponding to the cusps in the Bloch vector's path, i.e., when  $\cos(\omega t) = 0$ .

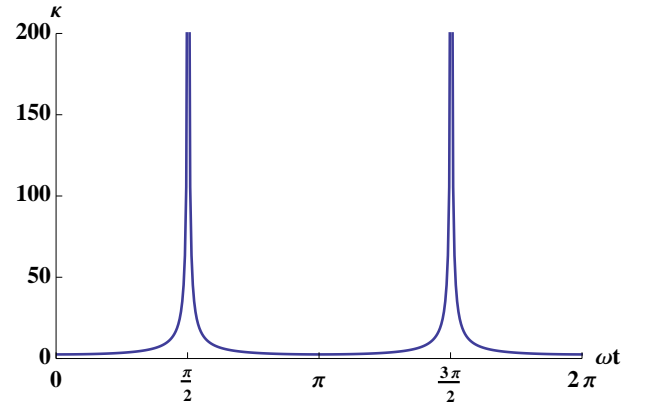


FIG. 7. Curvature  $\kappa$  versus rescaled time  $\omega t$ .

- 
- [1] G. Benenti, G. Casati, and G. Strini, *Principles of Quantum Computation and Information*, Vol. I: Basic concepts (World Scientific, Singapore, 2004); Vol. II: Basic tools and special topics (World Scientific, Singapore, 2007).
  - [2] M. A. Nielsen and I. L. Chuang, *Quantum computation and quantum information* (Cambridge University Press, Cambridge, 2000).
  - [3] P. Meystre and M. Sargent III, *Elements of quantum optics* (4th Ed.) (Springer-Verlag, Berlin, 2007).
  - [4] J. M. Raimond, M. Brune, and S. Haroche Rev. Mod. Phys. **73**, 565 (2001).
  - [5] A. Blais, R.-S. Huang, A. Wallraff, S. M. Girvin, and R. J. Schoelkopf, Phys. Rev. A **69**, 062320 (2004).
  - [6] A. Wallraff, D. I. Schuster, A. Blais, L. Frunzio, R.-S. Huang, J. Majer, S. Kumar, S. M. Girvin, and R. J. Schoelkopf, Nature **431**, 162 (2004).
  - [7] J. Bourassa, J. M. Gambetta, A. A. Abdumalikov, Jr., O. Astafiev, Y. Nakamura, and A. Blais, Phys. Rev. A **80**, 032109 (2009).
  - [8] T. Niemczyk, F. Deppe, H. Huebl, E. Menzel, F. Hocke, M. J. Schwarz, J. J. García-Ripoll, D. Zueco, T. Hümmer, E. Solano, A. Marx, and R. Gross, Nature Phys. **6**, 772 (2010).
  - [9] P. Forn-Díaz, J. Lisenfeld, D. Marcos, J. J. García-Ripoll, E. Solano, C. J. P. M. Harmans, and J. E. Mooij, Phys. Rev. Lett. **105**, 237001 (2010).
  - [10] M. S. Shahriar, P. Pradhan, and J. Morzinski, Phys. Rev. A **69**, 032308 (2004).
  - [11] E. K. Irish, J. Gea-Banacloche, I. Martin, and K. C. Schwab, Phys. Rev. B **72**, 195410 (2005).
  - [12] J. Casanova, G. Romero, I. Lizuain, J. J. García-Ripoll, and E. Solano, Phys. Rev. Lett. **105**, 263603 (2010).
  - [13] S. Ashhab and F. Nori, Phys. Rev. A **81**, 042311 (2010).
  - [14] J. Hausinger and M. Grifoni, Phys. Rev. A **82**, 062320 (2010).
  - [15] J. Hausinger and M. Grifoni, Phys. Rev. A **83**, 030301 (2011).

- [16] J. Hausinger and M. Grifoni, *New J. Phys.* **10**, 115015 (2008).
- [17] F. Beaudoin, J. M. Gambetta, and A. Blais, *Phys. Rev. A* **84**, 043832 (2011).
- [18] M. Bina, G. Romero, J. Casanova, J. J. García-Ripoll, A. Lulli, and E. Solano *Eur. Phys. J. Special Topics* **203**, 207 (2012).
- [19] For a derivation of Hamiltonian (1) see, for instance, Ref. [1], exercise 8.5 page 532, solution page 632.
- [20] The fact that the functions  $X(t)$ ,  $Y(t)$  and  $Z(t)$  are continuous and differentiable functions is a consequence of the Cauchy-Peano theorem applied to the first-order differential equations (2).
- [21] See, for instance, Ref. [1].
- [22] G. Benenti, S. Siccaldi, and G. Strini, in preparation.